Robust Mask Design with Defocus Variation Using Inverse Synthesis

Ningning Jia[a], Alfred K. Wong[b], and Edmund Y. Lam[a]

[a]Imaging Systems Laboratory, Department of Electrical and Electronic Engineering, The University of Hong Kong, Pokfulam Road, Hong Kong
[b]Magma Design Automation Inc., Santa Clara, CA 95054, USA

ABSTRACT

The continuous integrated circuit miniaturization and the shrinkage of critical dimension (CD) have pushed the development of optical proximity correction (OPC), and also making CD more sensitive to process variations. Traditional OPC optimizes mask patterns at nominal lithography conditions, which may lead to poor performance with process variations. Hence, OPC software nowadays needs to take different process conditions into consideration to enhance the robustness of layout patterns. In this paper, we propose an algorithm which considers the defocus as a random variable when incorporating it into an inverse imaging framework to optimize the input mask, in order to gain more robustness for a wider range of focus errors. The optimal mask is calculated in a statistical manner by minimizing the expected difference between output patterns at different defocus conditions and the target pattern. With the necessary tradeoff in the close proximity of the nominal focus condition, the optimized mask gives more robust performance under a wider range of focus errors.

Keywords: Optical proximity correction, inverse lithography, image synthesis, defocus

1. INTRODUCTION

Optical proximity correction (OPC) is a widely used resolution enhancement technique (RET) in optical lithography by modifying the mask patterns to improve printability. Rule-based OPC and model-based OPC are two main numerical correction approaches.[1] In rule-based OPC, correction is applied to features like edges, corners and interconnections, regulated by empirical rules or tables. Rule-based OPC is easy to implement, but it only improves nearest edges fidelity rather than in full optical interaction range.[2,3] Model-based OPC, which uses mathematical models to represent the fabrication process, calculates corrections globally.[4–6] In addition, it can be applied to different lithography conditions without obtaining stock of data beforehand.[3]

Most model-based OPC calculates solutions under nominal imaging conditions, without taking process variations into account. However, with the lower k_1 factor, printed critical dimensions (CD) become more sensitive to process variations, such as exposure dose variation and focus variation. As a result, process conditions deserve more attention and are being incorporated in OPC algorithms to enhance the robustness of printed patterns. Defocus aerial images have been considered to use in OPC software instead of best focus aerial images to improve focus latitude.[7–9] However, extensive simulation needs to be done to choose the appropriate defocus conditions.[7] A process variation aware OPC model (PVOPC) has been proposed later into OPC software to improve the robustness of post-OPC results with two main process variations, exposure variation and focus variation, and an analytical defocus aerial image expansion function has been derived.[10,11] This work focuses on edge placement error rather than global pattern fidelity. Recently, a continuous process window model has been developed to attain good performance both under nominal condition and with defocus and dose variations, in which focus variation is one of the continuous adjustable variables.[12]

In this paper, we aim to incorporate process variations into an inverse imaging synthesis framework for robust mask design. Similar to Ref. 13, pre-distorted mask design has been formulated as an image synthesis problem. On the basis of the inverse imaging system, this paper proposes a statistical algorithm with respect to the random focus variable to solve an optimization problem for a better global performance of layout patterns.

Further author information: (Send correspondence to Edmund Y. Lam)
Edmund Y. Lam: E-mail: elam@eee.hku.hk, Telephone: 852 2241-5942

Lithography Asia 2008, edited by Alek C. Chen, Burn Lin, Anthony Yen, Proc. of SPIE Vol. 7140, 71401W

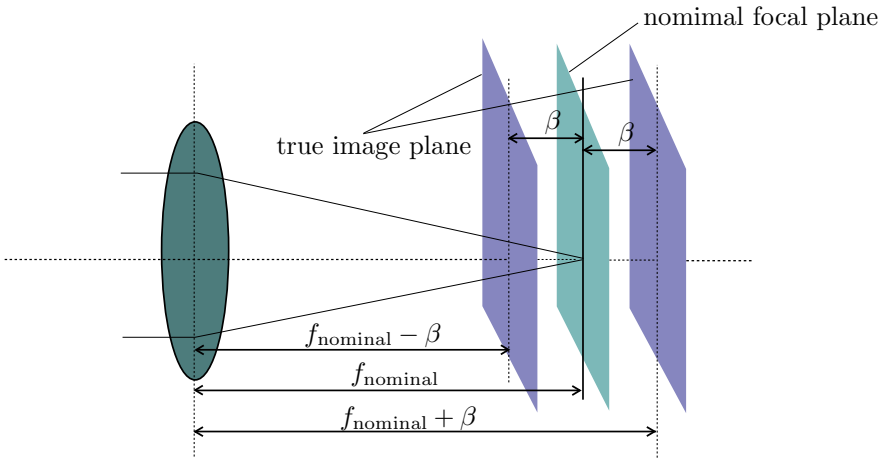

Figure 1. Defocus model

We choose a simple mathematical model to approximate the physical processes, including optical projection and photo-resist, and we assume a coherent imaging system. More sophisticated approximation models for different imaging systems such as Hopkins equations and Bessel functions can also be used in our framework with more computational complexity,[14] which will be further explored in the future. For the current work, we mainly want to illustrate the effectiveness of our proposed framework in designing robust optical mask with focus variation.

The rest of this paper is organized as follows. In Sec. 2, mathematical models and the structure of our algorithm are presented. In Sec. 3, experimental results are given with discussions to follow. Finally, Sec. 4 provides the conclusion.

2. MATHEMATICAL MODELS AND ALGORITHM STRUCTURE

The main idea of our algorithm is to consider focus error as a random variable, and then incorporate its statistical property into an optimization setting. The optimization aims to minimize the expected pattern fidelity difference between the printed pattern on the wafer under different defocus conditions and the target pattern. The input mask that gives rise to the minimum is considered the optimal design, which is expected to be robust against focus variation.

Before giving more mathematical details of our algorithm, we explain here the symbols used in the subsequent parts. Both optical projection and etching of the photo-resists are physical processes in the real world, which are approximated in our mathematical model by continuous functions. However, we use pixel-based representations in our implementation, which is discrete.[13] Thus, the input mask pattern, aerial image, output pattern and target pattern are all represented by 2D matrices, defined as M, I_{aerial}, I_{output}, and I_{target} with the same size $N \times K$ respectively. We use $\mathcal{E}$ to denote the expectation operator.

In optical lithography, the image plane does not always lie on the focal plane, but may vary randomly around it. In other words, the distance between image plane and the focal plane, which is defined as the focus error in this paper, behaves like a random variable, representing by symbol β. Fig. 1 shows a simplified defocus model. Nominal focal length f_{nominal} is measured by the distance from the lens center to the focal plane. If the true image plane is shorter, we have it as $f_{\text{nominal}} - \beta$; otherwise it is $f_{\text{nominal}} + \beta$. With defocus conditions being taken into consideration, the output pattern I_{output} is actually a function related to β. Details will be given later in this chapter.

Symbols used to represent other intermediate variables and functions will be clarified as they appear. The optimization problem we aim to solve is represented by

$$M_{\text{optimal}} = \arg\min_{M} \mathcal{E}\left\{ \|I_{\text{output}}(x,y;\beta) - I_{\text{target}}(x,y)\|_2^2 \right\}. \quad (1)$$

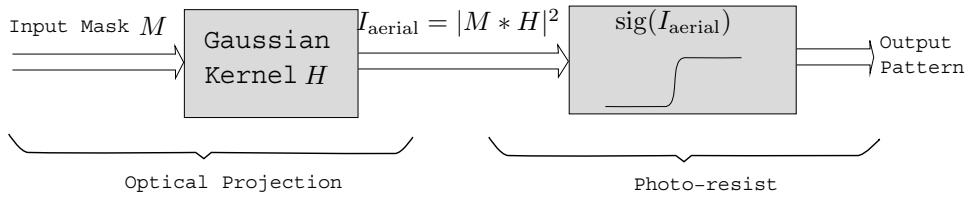

Figure 2. Forward model of the optical lithography system.

$I_{\text{output}}(x, y; \beta)$ and $I_{\text{target}}(x, y)$ take only binary values $\{0, 1\}$. L_2 norm is used here for the convenience of analytical calculation, although because both are binary-valued, L_1 and L_2 norm would give the same answer. In order to optimize the average performance of layouts, the objective function takes expectation of the difference under different off-focus conditions with a certain distribution of the random variable β. If we assume the mask $M(x, y)$ is a chromium-on-glass (COG) mask, which is also binary-valued, the optimization task can be described as

$$\begin{aligned} &\text{minimize} \quad \mathcal{E}\left\{ \|I_{\text{output}}(x, y; \beta) - I_{\text{target}}(x, y)\|_2^2 \right\} \\ &\text{subject to} \quad M(x, y) \in \{0, 1\}. \end{aligned} \tag{2}$$

Note that our work is not restricted to COG mask only. The same framework can also be applied to attenuated phase-shifting mask(PSM) where $M(x, y) \in \{-0.2646, 1\}$ or alternating PSMs where $M(x, y) \in \{-1, 0, 1\}$, although the last case would make the computation more challenging. In this paper we take COG as an example to prove the effectiveness of our algorithm. We need to express how $I_{\text{output}}(x, y; \beta)$ is related to $M(x, y)$. As mentioned the above, We divide the imaging model into optical projection and etching of the photo-resist. For the former, a Gaussian kernel is employed to approximate the amplitude spread function (ASF), with which the aerial images are calculated. In a coherent imaging system, Bessel kernel can be employed for a more precise description of the system. Here the Gaussian kernel is used to simplify the modeling. Instead of a Heaviside step function, the etching of the photo-resist can be modeled by a sigmoid function[13, 15]

$$\text{sig}(x) = \frac{1}{1 + e^{-a(x - t_{\text{r}})}}. \tag{3}$$

Given a threshold t_{r}, any region in aerial image with intensity higher than t_{r} will be developed. Variable a is a positive parameter determining the contrast of the sigmoid function. The complete forward lithography model is summarized in Fig. 2.

The system model described above works with nominal process conditions. However, in this work we take the focus variation into consideration as a random variable in the imaging system modeling. This is achieved by modifying the nominal ASF to a defocus-aware ASF. Let $H_0(x, y)$ denote the nominal ASF in a coherent imaging system, and $H(x, y; \beta)$ denote the modified ASF at defocus β. $\mathcal{F}$ denotes the Fourier transform. Defocus term is incorporated into the ASF by multipling an exponential term in the frequency domain, i.e.[14, 16]

$$\mathcal{F}\{H\}(u, v; \beta) = \mathcal{F}\{H_0\}(u, v) \times e^{-j\pi(u^2 + v^2)\beta} \tag{4}$$

where $j = \sqrt{-1}$, and u and v denote the spatial frequencies.

For brevity in description we introduce the term $E(x, y; \beta) = M(x, y) * H(x, y; \beta)$. Then, the aerial image I_{aerial} is represented by

$$I_{\text{aerial}}(x, y; \beta) = |E(x, y; \beta)|^2 = |M(x, y) * H(x, y; \beta)|^2. \tag{5}$$

Then, the output image with focus error β is

$$I_{\text{output}}(x, y; \beta) = \frac{1}{1 + e^{-a\left(I_{\text{aerial}}(x, y; \beta) - t_{\text{r}}\right)}}. \tag{6}$$

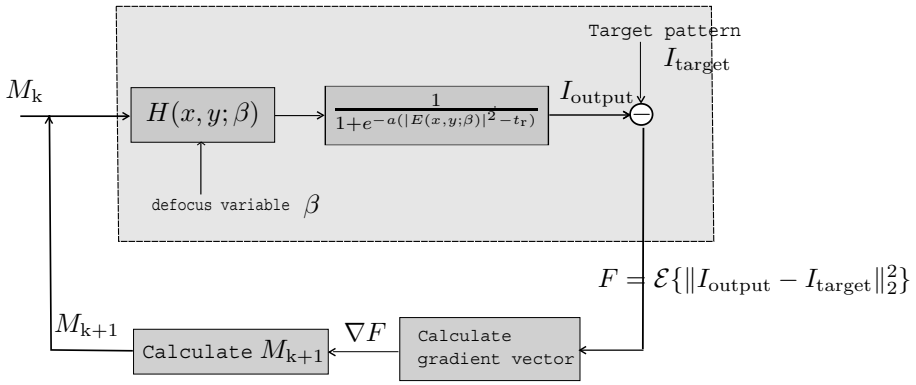

Figure 3. The optimization framework.

2.1 Optimization

As with many model-based OPC methods, the corrections are calculated iteratively until the distance between the output image and the target image is minimized to reach certain criteria in our work. The iterative optimization framework is illustrated in Fig. 3.

Equation 2 stipulates that $M(x,y) \in \{0,1\}$, which renders the above a combinatorial optimization problem. One common approach is to relax the constraint $M(x,y) \in \{0,1\}$ to $0 \le M(x,y) \le 1$, and employ a gradient-based algorithm for the iterations.[17] The first step is to calculate the gradient vector of cost function, which we call F, and can be written as

$$\begin{aligned} F &= \mathcal{E}\left\{\sum_x \sum_y \left[I_{\text{output}}(x,y;\beta) - I_{\text{target}}(x,y)\right]^2\right\} \\ &= \mathcal{E}\left\{\sum_x \sum_y \left[\frac{1}{1+e^{-a(|E(x,y;\beta)|^2-t_{\text{r}})}} - I_{\text{target}}(x,y)\right]^2\right\}. \end{aligned} \tag{7}$$

As $E(x,y;\beta)$ and $H(x,y;\beta)$ are in general complex, for the derivations below we divide them into real and imaginary parts respectively, i.e.

$$E(x,y;\beta) = E_{\text{real}}(x,y;\beta) + jE_{\text{img}}(x,y;\beta) \tag{8}$$

$$H(x,y;\beta) = H_{\text{real}}(x,y;\beta) + jH_{\text{img}}(x,y;\beta). \tag{9}$$

With these, Equation 7 can be written as

$$F = \mathcal{E}\left\{\sum_x \sum_y \left[\frac{1}{1+e^{-a\left(E^2_{\text{real}}(x,y;\beta)+E^2_{\text{img}}(x,y;\beta)-t_{\text{r}}\right)}} - I_{\text{target}}(x,y)\right]^2\right\}. \tag{10}$$

We break up the amplitude into two parts and calculate the derivative respectively in order to avoid the absolute operation. The gradient vector is calculated as

$$\begin{aligned} \nabla F &= 2a \times \mathcal{E}\Big\{H_{\text{real}}(\beta) * \left[\left(I_{\text{output}}(\beta) - I_{\text{target}}\right) \bullet I_{\text{output}}(\beta) \bullet \left(1 - I_{\text{output}}(\beta)\right) \bullet E_{\text{real}}(\beta)\right] \\ &\quad + H_{\text{img}}(\beta) * \left[\left(I_{\text{output}}(\beta) - I_{\text{target}}\right) \bullet I_{\text{output}}(\beta) \bullet \left(1 - I_{\text{output}}(\beta)\right) \bullet E_{\text{img}}(\beta)\right]\Big\} \end{aligned} \tag{11}$$

where $\bullet$ denotes the element-by-element multiplication. Its derivation is given in Appendix A.

Equation 11 is calculated to update the mask pattern that we aim to optimize in each step of the iterative algorithm. It includes not only the difference between the output and the target pattern as well as the distortion

due to diffraction, but also the average amount of change under different defocus conditions by employing the expectation operator. Thus, it optimizes the mask pattern over the defocus range, which tends to be more robust to off-focus fluctuation than an optimization at the nominal conditions only.

We choose steepest descent as the gradient method in this paper.[13,15] The update for $(k+1)$ iteration is given by

$$M^{(k+1)}(x,y) = M^{(k)}(x,y) - s \times \frac{\nabla F(x,y)}{\|\nabla F(x,y)\|}, \tag{12}$$

where s is the step size. Moreover, we enforce the constraints with an active set algorithm. This method projects all out-of-bound variables to their closest bound.[17,18] Thus, for every $M(x,y) < 0$, we set $M(x,y) = 0$. Likewise, we set $M(x,y) = 1$ when $M(x,y) > 1$. After a number of searching steps, the iteration can be stopped when the value of the cost function has decreased below a certain threshold value. The input mask whose output gives the shortest distance with the target pattern is considered to be the optimal mask.

3. RESULTS AND DISCUSSIONS

We employ the inverse imaging method to design some Chromium-on-glass (COG) mask patterns, where $M(x,y) \in \{0,1\}$, which are robust against focus fluctuations. System parameters are set as follows: $\lambda = 193$nm, $NA = 0.85$, resolution=10nm/pixel, thresholding $t_r = 0.3$. Fig. 4 shows the results for the two-rectangle pattern.

We construct the optimal masks targeted for the nominal conditions only by employing the algorithm in Ref. 13, and compare the results with the outputs generated by our algorithm. In Fig. 4, (a) is the target pattern, (b) is the optimal mask using the method of Ref. 13, (c) is our optimal mask, (d) and (f) are the output patterns under infocus and 160nm focus error respectively with (b) as the input, while (e) and (g) are the outputs with (c) as the input. We see that under 160nm defocus, our algorithm can still maintain the separation of the two rectangles, while we lose a little in the ideal focus condition compared to the nominal optimal mask in (b). This pattern fidelity loss is predictable, because the expectation operation tends to compensate and cancel the distortion brought by different defocus conditions on the input mask pattern. Fig. 5 plots the performance of our algorithm versus optimization only under nominal conditions. The performance is measured by calculating the distance (pixel error) between the output patterns and the target pattern under a set of evenly sampled defocus values. We sample in the range of $(-400\text{nm}, 400\text{nm})$, since focus error larger than this range appears unlikely. Fig. 5 shows that the performance of our algorithm (represented by the green line) excels in the defocus range of $(-320\text{nm}, -120\text{nm}) \bigcap (120\text{nm}, 320\text{nm})$. Actually, our algorithm can maintain the separation of the two rectangles up to 200nm defocus, compared with 120nm for the other method.

The test results of the other two patterns are shown in Fig. 6 and Fig. 8 respectively. Likewise, Fig. 7 and Fig. 9 draw the comparison of our method's performance with the optimal mask generated under nominal conditions. These two patterns show less sensitivity to focus fluctuation, especially pattern #2. This is attributed in part to the simplified model we use, which may not be able to simulate the real physical defocus phenomenon accurately enough. It may also be possible that the distortion brought by diffraction overwhelms the focus error for some patterns. Thus, the optimal masks designed under nominal focus conditions tend to have acceptable performance with a small range of defocus. Nevertheless, from Fig. 8, we could see some small patterns (contacts) still connecting with each other in (h), while in (i) the contacts remain separate from each other. Note that (h) and (i) are outputs of (b) and (c) under the same focus error $300nm$ respectively. In addition, our result at in-focus (shown in (e)) has little loss in fidelity compared to (d), the nominal output pattern.

4. CONCLUSION

In this paper, an algorithm incorporating statistical variations of image focus into an inverse imaging system is proposed. Results show that our optimal mask performs better in certain range of off-focus values, with some trade-off at the nominal conditions. We are currently updating our algorithm in the following aspects. For the system modeling, more sophisticated and precise mathematical models are used to simulate the physical lithography process. We also aim to improve the algorithm so that it takes into account the varied requirement for error margin with different parts of the circuit. Finally, to improve on the speed, gradient descent method can be substituted by conjugate gradient for fast convergence.[17,19]

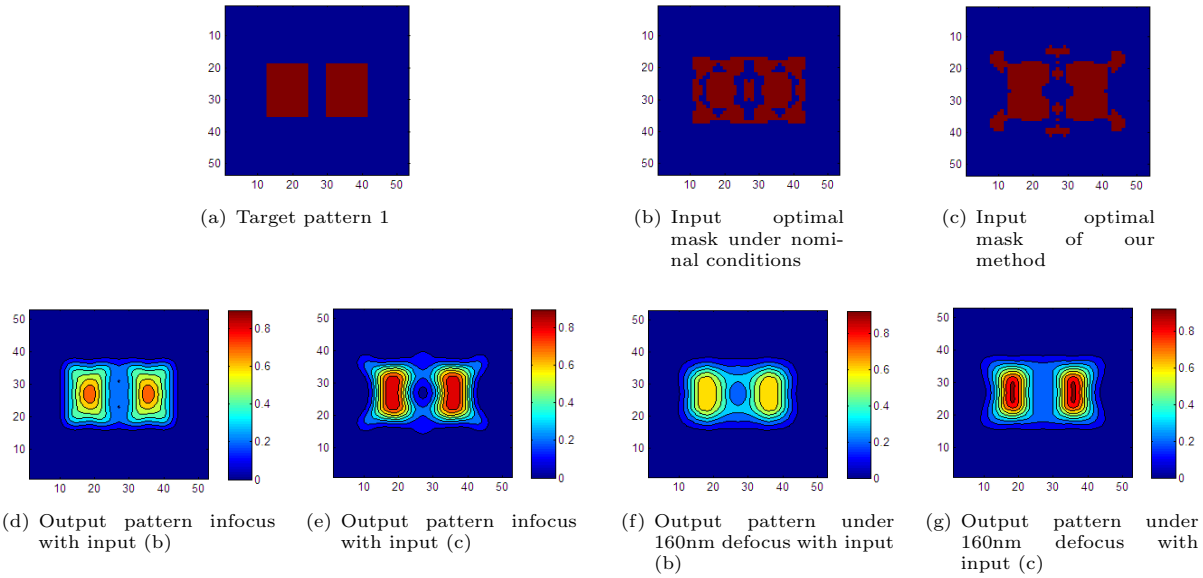

(a) Target pattern 1

(b) Input optimal mask under nominal conditions

(c) Input optimal mask of our method

(d) Output pattern infocus with input (b)

(e) Output pattern infocus with input (c)

(f) Output pattern under 160nm defocus with input (b)

(g) Output pattern under 160nm defocus with input (c)

Figure 4. Experimental results for a two-rectangle pattern.

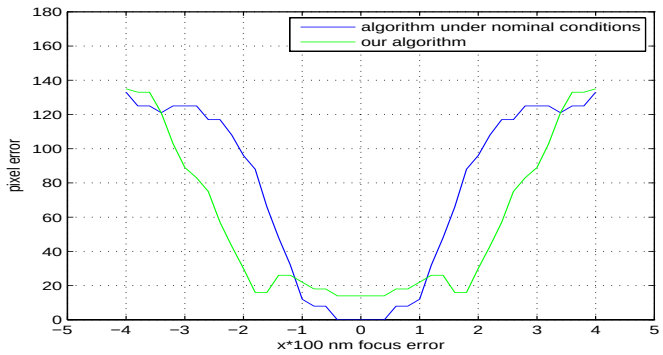

Figure 5. Comparison of pixel errors under different focus errors.

ACKNOWLEDGMENTS

The work described in this paper was partially supported by two grants from the Research Grants Council of the Hong Kong Special Administrative Region, China (Project Numbers 713906 and 713408).

APPENDIX A. DERIVATION OF GRADIENT

Given the cost function

$$\mathrm{F} = \mathcal{E}\left\{ \|I_{\text{output}}(x,y;\beta) - I_{\text{target}}\|_2^2 \right\},$$

we derive the gradience ∇F as follows:

$$\begin{aligned} F &= \mathcal{E}\left\{ \sum_{x=1}^{N}\sum_{y=1}^{K} \left[I_{\text{output}}(x,y;\beta) - I_{\text{target}}(x,y)\right]^2 \right\} \\ &= \mathcal{E}\left\{ \sum_{x=1}^{N}\sum_{y=1}^{K} \left[I_{\text{output}}^2(x,y;\beta) - 2I_{\text{output}}(x,y;\beta)I_{\text{target}}(x,y) + I_{\text{target}}^2(x,y)\right] \right\}. \end{aligned} \tag{13}$$

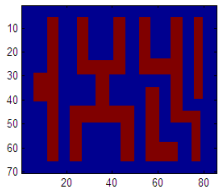

(a) Target pattern 2

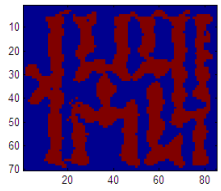

(b) Input optimal mask under nominal conditions

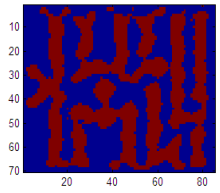

(c) Input optimal mask of our method

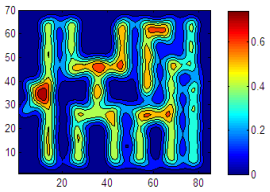

(d) Output pattern infocus with input (b)

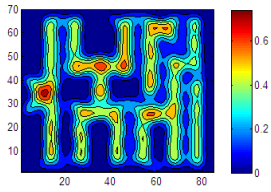

(e) Output pattern infocus with input (c)

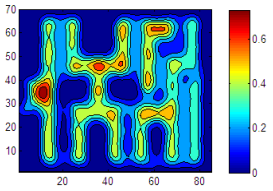

(f) Output pattern under 220nm defocus with input (b)

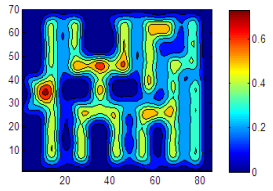

(g) Output pattern under 220nm defocus with input (c)

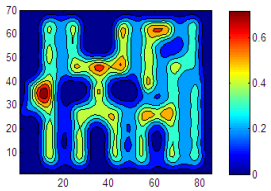

(h) Output pattern under 300nm defocus with input (b)

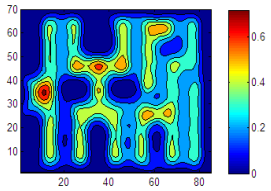

(i) Output pattern under 300nm defocus with input (c)

Figure 6. Experimental results for pattern #2.

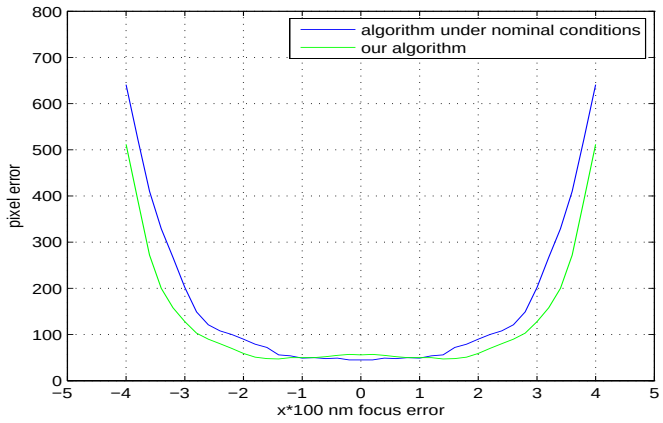

Figure 7. Comparison of pixel errors under different focus errors.

Therefore,

$$\frac{\partial F(x,y;\beta)}{\partial M(p,q)} = \mathcal{E}\left\{\sum_{x=1}^{N}\sum_{y=1}^{K}\left[\left(2I_{\text{output}}(x,y;\beta)-2I_{\text{target}}(x,y)\right)\frac{\partial I_{\text{output}}(x,y;\beta)}{\partial M(p,q)}\right]\right\}$$

$$
\begin{aligned}
&= \mathcal{E}\left\{\sum_{x=1}^{N}\sum_{y=1}^{K}\left[\big(2I_{\text{output}}(x,y;\beta)-2I_{\text{target}}(x,y)\big)\frac{\partial\frac{1}{1+e^{-a(|E(x,y;\beta)|^2-t_r)}}}{\partial M(p,q)}\right]\right\}\\
&= \mathcal{E}\left\{\sum_{x=1}^{N}\sum_{y=1}^{K}\big(2I_{\text{output}}(x,y;\beta)-2I_{\text{target}}(x,y)\big)(-a)\left(\frac{1}{1+e^{-a(|E(x,y;\beta)|^2-t_r)}}\right)\right.\\
&\qquad\left.\times\left(1-\frac{1}{1+e^{-a(|E(x,y;\beta)|^2-t_r)}}\right)\frac{\partial|E(x,y;\beta)|^2}{\partial M(p,q)}\right\}. \qquad (14)
\end{aligned}
$$

As mentioned above, the modified ASF is complex because the exponential defocus term introduces extra phases into the nominal ASF. In a coherent system, the aerial image is in fact the amplitude of a complex matrix. Thus we break $E(x,y;\beta)$ into its real part and imaginary part, and represent the aerial image by

$$
I_{\text{aerial}}(x,y;\beta)=|E(x,y;\beta)|^2=E^2_{\text{real}}(x,y;\beta)+E^2_{\text{img}}(x,y;\beta). \qquad (15)
$$

We then calculate the differentiation separately as

$$
\begin{aligned}
\frac{\partial F(x,y;\beta)}{\partial M(p,q)} &= \mathcal{E}\left\{\sum_{x=1}^{N}\sum_{y=1}^{K}\left[\big(2I_{\text{output}}(x,y;\beta)-2I_{\text{target}}(x,y)\big)(-a)\left(\frac{1}{1+e^{-a(|E(x,y;\beta)|^2-t_r)}}\right)\right.\right.\\
&\qquad\left.\left.\times\left(1-\frac{1}{1+e^{-a(|E(x,y;\beta)|^2-t_r)}}\right)\frac{\partial\big(E^2_{\text{real}}(x,y;\beta)+E^2_{\text{img}}(x,y;\beta)\big)}{\partial M(p,q)}\right]\right\}\\
&= \mathcal{E}\left\{\sum_{x=1}^{N}\sum_{y=1}^{K}\big(2I_{\text{output}}(x,y;\beta)-2I_{\text{target}}(x,y)\big)(-a)\left(\frac{1}{1+e^{-a(|E(x,y;\beta)|^2-t_r)}}\right)\right.\\
&\qquad\times\left(1-\frac{1}{1+e^{-a(|E(x,y;\beta)|^2-t_r)}}\right)2\left(E_{\text{real}}(x,y;\beta)\frac{\partial E_{\text{real}}(x,y;\beta)}{\partial M(p,q)}\right.\\
&\qquad\left.\left.+E_{\text{img}}(x,y;\beta)\frac{\partial+E_{\text{img}}(x,y;\beta)}{\partial M(p,q)}\right)\right\}\\
&= \mathcal{E}\left\{\sum_{x=1}^{N}\sum_{y=1}^{K}\big(2I_{\text{output}}(x,y;\beta)-2I_{\text{target}}(x,y)\big)(-a)\left(\frac{1}{1+e^{-a(|E(x,y;\beta)|^2-t_r)}}\right)\right.\\
&\qquad\times\left(1-\frac{1}{1+e^{-a(|E(x,y;\beta)|^2-t_r)}}\right)2\big(E_{\text{real}}(x,y;\beta)H_{\text{real}}(x-p,y-q;\beta)\\
&\qquad\left.+E_{\text{img}}(x,y;\beta)H_{\text{img}}(x-p,y-q;\beta)\big)\right\}\\
&= 2a\times\mathcal{E}\Big\{H_{\text{real}}(x,y;\beta)*\big[\big(I_{\text{output}}(x,y;\beta)-I_{\text{target}}(x,y)\big)I_{\text{output}}(x,y;\beta)\big(1-I_{\text{output}}(x,y;\beta)\big)\\
&\qquad\times E_{\text{real}}(x,y;\beta)\big]+H_{\text{img}}(x,y;\beta)*\big[\big(I_{\text{output}}(x,y;\beta)-I_{\text{target}}(x,y)\big)I_{\text{output}}(x,y;\beta)\\
&\qquad\times\big(1-I_{\text{output}}(x,y;\beta)\big)E_{\text{img}}(x,y;\beta)\big]\Big\}. \qquad (16)
\end{aligned}
$$

Equation (16) can be formulated using matrix as follows:

$$
\begin{aligned}
\nabla F &= 2a\times\mathcal{E}\Big\{H_{\text{real}}(\beta)*\big[\big(I_{\text{output}}(\beta)-I_{\text{target}}\big)\bullet I_{\text{output}}(\beta)\bullet\big(1-I_{\text{output}}(\beta)\big)\bullet E_{\text{real}}(\beta)\big]\\
&\qquad+H_{\text{img}}(\beta)*\big[\big(I_{\text{output}}(\beta)-I_{\text{target}}\big)\bullet I_{\text{output}}(\beta)\bullet\big(1-I_{\text{output}}(\beta)\big)\bullet E_{\text{img}}(\beta)\big]\Big\}. \qquad (17)
\end{aligned}
$$

REFERENCES

1. A. K. Wong, *Resolution Enhancement Techniques in Optical Lithography*, SPIE, Washington, 2001.

2. O. W. Otto, J. G. Garofalo, K. Low, C.-M. Yuan, R. C. Henderson, C. Pierrat, R. L. Kostelak, S. Vaidya, and P. Vasudev, "Automated optical proximity correction: a rules-based approach," in *Optical Microlithography*, *Proc. SPIE* **2197**, pp. 278–293, 1994.
3. S. Shioiri and H. Tanabe, "Fast optical proximity correction: Analytical method," in *Pattern Proximity Correction II*, *Proc. SPIE* **2440**, pp. 261–269, 1995.
4. N. Cobb and A. Zakhor, "Fast, low-complexity mask design," in *Optical Microlithography*, *Proc. SPIE* **2440**, pp. 313–327, 1995.
5. S. Sherif, B. Salehand, and R. De Leone, "Binary image synthesis using mixed linear integer programming," *IEEE Trans. Image Process* **4**, pp. 1252–1257, 1995.
6. Y. Liu and A. Zakhor, "Binary and phase shifting mask design for optical lithography," *IEEE Trans. Semiconductor Manufacturing* **5**, pp. 138–152, 1992.
7. J. L. Sturtevant, J. A. Torres, J. Word, and P. L. Y. Granik, "Consideration for the use of defocus models for OPC," in *Design and Process Integration for Microelectronic Manufacturing III*, L. W. Liebmann, ed., *Proc. SPIE* **5756**, 2005.
8. N. B. Cobb and Y. Granik, "OPC methods to improve image slope and process window," in *Design and Process Integration for Microelectronic Manufacturing II*, A. Starikov, ed., *Proc. SPIE* **5042**, 2003.
9. Q. Qian, "Focus latitude optimization for model based opc," in *Annual BACUS Symposium on Photomask Technology*, K. R. Kimmel, ed., *Proc. SPIE* **5256**, 2003.
10. P. Yu, D. Z. Pan, and C. A.Mack, "Fast lithography simulation under focus variations for OPC and layout optimizations," in *Design and Process Integration for Microelectronic Manufacturing IV*, A. K. K. Wong, ed., *Proc. SPIE* **6156**, 2006.
11. P. Yu, S. X. Shi, and D. Z. Pan, "True process variation aware optical proximity correction with variational lithography modeling and model calibration," *J. Micro/Nanolith. MEMS MOEMS* **6**, p. 031004, 2007.
12. Q. Zhang, Q. Yan, Y. Zhang, and K. Lucas, "Continuous process window modeling for process variation aware OPC and lithography verification," in *Design for Manufacturability through Design-Process Integration II*, V. K.Singh, ed., *Proc. SPIE* **6925**, pp. 458–467, 2008.
13. A. Poonawala and P. Milanfar, "Mask design for optical microlithography — An inverse imaging problem," *IEEE Trans. Image Process.* **16**, pp. 774–788, 2007.
14. J. W. Goodman, *Introduction to Fourier Optics*, Roberts & Company, Greenwood Village, 2005.
15. X. Ma and G. R. Arce, "Generalized inverse lithography methods for phase-shifting mask design," in *Optical Microlithography XX*, D. G. Flagello, ed., *Proc. SPIE* **6520**, 2007.
16. S. Förster, H. Gross, F. Höller, L. Höring, and C. Zeiss, "Extended depth of focus as a process of pupil manipulation," in *Optical Design and Engineering II*, L. Mazuray and R. Wartmann, eds., *Proc. SPIE* **5962**, p. 596202, 2005.
17. S. H. Chan, A. K. Wong, and E. Y. Lam, "Initialization for robust inverse synthesis of phase-shifting masks in optical projection lithography," *Optics Express* **16**, pp. 14746–14760, 2008.
18. P. E. Gill, W. Murray, and M. H. Wright, *Practical Optimization*, Academic Press, London, 1986.
19. M. Michel, *Mathematical Programming : Theory and Algorithms*, Wiley, Chichester, 1986.

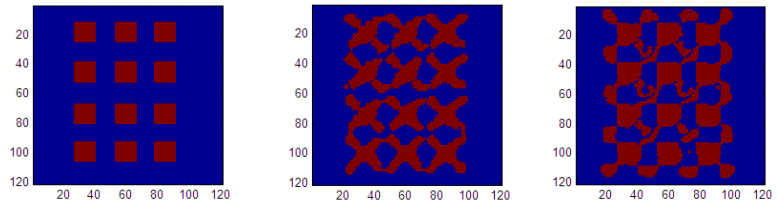

(a) Target pattern 3 (b) Input optimal mask under nominal conditions (c) Input optimal mask of our method

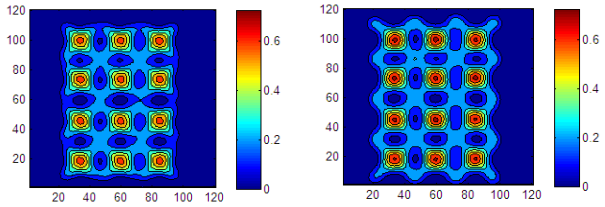

(d) Output pattern infocus with input (b) (e) Output pattern infocus with input (c)

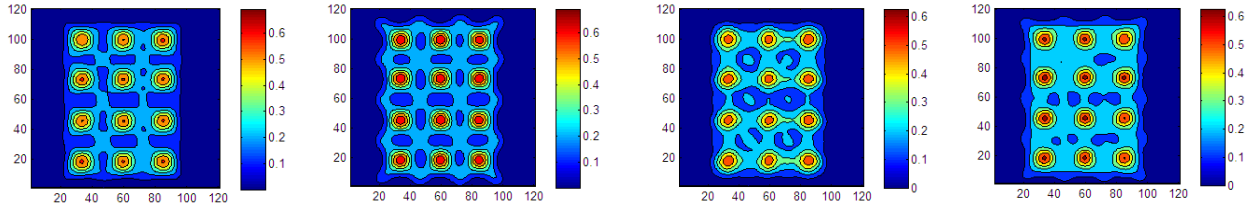

(f) Output pattern under 200nm defocus with input (b) (g) Output pattern under 200nm defocus with input (c) (h) Output pattern under 300nm defocus with input (b) (i) Output pattern under 300nm defocus with input (c)

Figure 8. Experimental results for pattern #3.

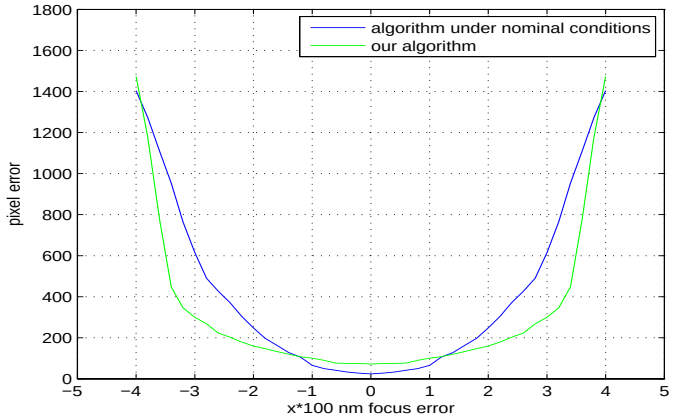

Figure 9. Comparison of pixel errors under different focus errors.